Activation of regenerated CoMo/Al2O3 hydrotreating catalysts by organic additives - The particular case of maleic acid

?. Ngoc-Quynh Bui, C. Geantet, G. Berhault

Activation of Regenerated $CoMo/Al_2O_3$ Hydrotreating Catalysts by Organic Additives – The Particular Case of Maleic Acid

Ngoc-Quynh Bui, Christophe Geantet, Gilles Berhault*

Institut de Recherches sur la Catalyse et l'Environnement de Lyon,
CNRS – Université Lyon I, 02 avenue Albert Einstein, 69100 Villeurbanne, France

All correspondence should be sent to Gilles Berhault:

Ph: (+33) 472 44 54 43

Fax: (+33) 472 44 53 99

E-mail: Gilles.Berhault@ircelyon.univ-lyon1.fr

Abstract

Activation of hydrodesulfurization (HDS) catalysts through sulfidation of oxide precursors is a critical procedure required to achieve preparation of the Co(Ni)-promoted $Mo(W)S_2$ sulfides commonly used for performing sulfur removal from transportation fuels. Better optimized preparation of HDS catalysts can be reached if organic additives, glycol-type compounds or chelating agents, are used during the activation process. Moreover, comprehension of the role of the organic additives during activation has become even more essential with the increasing necessity to regenerate satisfactorily the last generation of HDS catalysts, more sensitive to the harsh conditions used during the oxidative regeneration treatment. In this respect, maleic acid (MA) was recently found to be an efficient additive for the activation of regenerated HDS catalysts.

In the present study, deeper understanding of the role played by maleic acid for restoring the HDS activity was determined at different steps of the preparation of a regenerated CoMo-Al_2O_3 (here called CoMo-R) catalyst. Comparison was first performed to two other additives, a chelating agent, ethylenediaminetetraacetic acid (EDTA) and a glycol-type compound, triethyleneglycol (TEG), after impregnation and drying steps, using UV-vis diffuse reflectance spectroscopy, ex situ and in situ X-ray diffraction and thermal analysis. Results emphasized that maleic acid is the most efficient additive for extracting cobalt from cobalt molybdate species leading after sulfidation to much better HDS catalytic properties in the HDS of 4,6-dimethyldibenzothiophene (4,6-DMDBT) and of a straight run gasoil.

The sulfidation step was also carefully analyzed during the activation of CoMo-R in the presence of MA using inductively coupled plasma atomic emission spectroscopy (ICP-AES), X-ray photoelectron, Raman and electron paramagnetic resonance spectroscopies, mass spectrometry analysis and transmission electron microscopy. This detailed analysis allows

proposing a complete description of the sulfidation mechanism in the presence of MA leading to a better understanding of the key aspects to be reached during the activation process.

Keywords

MoS_2; cobalt promotion; activation; maleic acid; regeneration.

1. Introduction

Sulfur-containing molecules naturally present in petroleum feedstock are harmful and poisoning compounds for post-combustion devices used in transportation vehicles for reducing emission of pollutants. For this reason, hydrodesulfurization (HDS) reactions performed in refineries for removing sulfur remain key processes for limiting atmospheric pollution. Continuous effort is then devoted to the preparation of more and more efficient HDS catalysts in order to respect current stringent environmental regulations applied worldwide [1]. Hydrodesulfurization catalysts are made of molybdenum (tungsten) sulfide slabs whose edge planes are promoted by cobalt or nickel. Their activation from an oxide precursor to their final sulfide phase is a critical step depending on multiple parameters influencing the nature of the oxide species formed and their evolution through sulfidation into active components [2, 3].

Addition of organic additives is now recognized as an efficient way to optimize the preparation of HDS catalysts [4-12]. Two main groups of additives were initially considered for the activation of MoS_2-based catalysts: glycol-type agents and chelating compounds (mainly aminopolycarboxylic acids). However, according to literature data, their respective role towards activation differs completely. Glycol-type agents (like polyethyleneglycol, PEG or triethyleneglycol, TEG) would help to redisperse Mo and Co species through probably the formation of heteropolymolybdates species containing also cobalt. Redispersion and close proximity of Co and Mo would then favor the formation of the so-called promoted CoMoS phase after sulfidation [13-16]. In the case of chelating agents based on aminopolycarboxylic acids (mainly nitrilotriacetic acid, NTA or ethylenediaminetetraacetic acid, EDTA), complexation occurs between the cobalt or nickel and the organic additive leading to a better accommodation of the promoters onto the MoS_2 edge planes [17-23]. The sulfidation of promoter atoms would then be delayed optimizing the location of Co or Ni on already-formed

MoS_2 slabs. However, this explanation was also questioned. Mazoyer et al. [24] showed that the addition of EDTA to $CoMo/Al_2O_3$ did not lead to an improved HDS activity due to delayed sulfidation of cobalt but rather to a selective Co extraction from inactive cobalt molybdate, $CoMoO_4$ precursor species leading to a better use of cobalt for accommodating molybdenum sulfide. Similarly, Van Haandel et al. [25] did not observe correlation between HDS catalytic activity and delayed cobalt sulfidation.

Another significant group of organic additives, α-hydroxycarboxylic acid, such as citric acid (CA), has been recently considered for optimizing the formation of the sulfide promoted $Co(Ni)/MoS_2$ phase [26-32]. However, its exact role during activation is unclear. Klimov et al. [30] initially proposed that citric acid would interact with both Mo and Co forming a $Co_2[Mo_4(C_6H_5O_7)_2O_{11}]$ complex. This assumption was not supported by more recent studies [25, 32]. Van Haandel et al. [25] concluded that citric acid was only chelated to cobalt. On the opposite, Chen et al. [32] did not observe Co-CA but Mo-CA complex. Van Haandel et al. [25] emphasized a more beneficial role of CA than EDTA for activating $CoMo/Al_2O_3$ catalysts and they attributed it to the weaker interaction of Co with the alumina support allowing its sulfidation at low temperature. CA would also favor the formation of more polymerized polymolybdates interacting weakly with the support and therefore leading to an easier Mo sulfidation. The concomitant low temperature regions for Co and Mo sulfidation would be the main parameter affecting the final catalytic activity. Chen et al. [32] concluded differently by considering the influence of CA on the final morphology of MoS_2 slabs. CA would favor the formation of S-edge slabs more akin to accommodate Co. However, this assumption was not supported by Afanasiev [33] who did not observe any significant influence of CA on the MoS_2 slab morphology.

Another important issue to consider is the activation of regenerated HDS catalysts. Due to coke formation and poisoning by contaminants naturally present in the feedstock to be treated

(V, Ni, As, Na), MoS_2-based catalysts tend to deactivate with time on stream. Each year, 25,000-30,000 tons of hydrotreating catalysts have to be regenerated. The regeneration process consists in an oxidative treatment at 450-550°C burning the carbon deposits and leading to a dispersed oxide phase. However, the most recent HDS catalysts cannot be restored to a sufficient catalytic activity level after regeneration (60-85% recovery vs 90+ % necessary) [34, 35].

In this respect, in our previous study, the use of another type of organic additive, an unsaturated dicarboxylic acid, maleic acid (MA) was considered for activating regenerated $CoMo/Al_2O_3$ catalysts [36]. Results showed that maleic acid was quite effective in consuming cobalt molybdate, $CoMoO_4$ formed during the regeneration step, by extracting selectively Co forming cobalt maleate, $Co(C_4H_3O_4)_2.4H_2O$. Mo initially present in $CoMoO_4$ is then redispersed forming Anderson $Al(OH)_6Mo_6O_{18}^{3-}$ moieties easily sulfided at low temperature. The cobalt maleate compound remains stable up to 300°C delaying the Co release until 350°C, temperature at which the promoter atoms can be efficiently accommodated onto the already formed MoS_2 slabs. Similarly, Budukva et al. [37] confirmed recently the interest of using chelating agents, particularly, α-hydroxycarboxylic acids, for partly restoring the activity of regenerated $CoMo/Al_2O_3$ catalysts.

However, the exact way maleic acid influences the sulfidation of $CoMo/Al_2O_3$ catalysts remains to be demonstrated. Moreover, its respective beneficial effect compared to other classical organic additives has not been reported yet. Therefore, the objective of the present study will be to compare maleic acid to two kind of organic additives, a chelating agent (EDTA) and a glycol-type agent (TEG) 1) during the impregnation, maturation and drying steps and 2) in terms of HDS efficiency through the determination of their respective activities for the conversion of a refractive to be desulfurized compound, 4,6-dimethyldibenzothiophene (4,6-DMDBT) and for the sulfur removal for a SRGO (straight run

gas oil) cut. The most active organic additive, maleic acid, will then be extensively characterized during the sulfidation of a regenerated $CoMo/Al_2O_3$ catalyst to provide a clear understanding of its role during the activation process.

2. Experimental

2.1. Preparation of the Different Catalysts Activated by MA, TEG or EDTA

The regenerated catalyst used here is a $CoMo/Al_2O_3$, called afterwards CoMo-R with 3.1 wt% Co and 13.8 wt% Mo. Specific surface areas (S_{BET}) and pore volumes are respectively 185 m^2/g and 0.42 cm^3/g. Before impregnation, CoMo-R was dried at 300°C under air for 2 h.

Optimized procedures of activation of the different additives were used herein in order to get differences only ascribed to the nature of each organic compound used. In the case of the diammonium salt of the ethylenediamine tetraacetic acid (diA-EDTA, simplified as EDTA afterwards), incipient wetness impregnation onto CoMo-R was performed using an optimized EDTA/(Co+Mo) molar ratio of 0.22. After impregnation, maturation was done at 90°C for 10 h before being dried at 120°C for 10 h [24].

In the case of triethyleneglycol (TEG), the protocol developed by Nguyen et al. [15] was followed. TEG was added to CoMo-R using an impregnation in excess method with a TEG/(Co+Mo) molar ratio of 0.5. Maturation was performed at room temperature (RT) for 12 h. The drying step was carried out at 100°C for 12 h under static air.

Using maleic acid, incipient wetness impregnation was done using an optimized MA/(Co+Mo) molar ratio of 0.44 (equivalent to MA/Co molar ratio of 1.6). The catalyst was then maturated at 60°C for 17 h before being dried under N_2 at 130°C [36].

For comparison purposes, cobalt maleate, $Co(C_4H_3O_4)_2.4H_2O$ was also synthesized using the procedure developed by Allan et al. [38]. First, 2.5 g of cobalt carbonate, $CoCO_3$ was progressively added to a 0.3 M maleic acid aqueous solution in order to obtain an MA/Co

molar ratio of 2.0. The final pH then reached a value of 2.3 higher than the first pKa value of maleic acid (1.8). $C_4H_3O_4^-$ species are therefore present in solution. The final solid is therefore retrieved by filtration and slow evaporation at RT for one week. XRD pattern of the final product is compared Figure S1, supporting information, with the JCPDS card 00-054-1724 of $Co(C_4H_3O_4)_2.4H_2O$ showing that cobalt maleate was effectively obtained here with a high purity.

2.2. Characterization Techniques

Elemental amounts of Mo and Co were determined by inductively coupled plasma – atomic emission spectroscopy (ICP-AES, Activa-Horiba Jobin Yvon). C and S amounts were obtained using a total combustion technique (CS-mat 5500 analyzer, Ströhlein Instruments).

X-ray diffraction analyses were performed using both ex situ and in situ techniques. For the ex situ experiments, a BRUKER D5005 or D8 ADVANCE A25 was used in the 3-80° 2θ range with Cu Kα radiation (λ=1.542 Å). In situ experiments were performed using a PANalytical XPERT MPD Pro diffractometer, an X'Celerator detector and an Anton Paar XRK 900 heating chamber. DIFFRAC.EVA and HighScore softwares were employed to determine crystalline phases.

Ultraviolet-visible diffuse reflectance spectra (UV-vis DR) were acquired in the 200-1100 nm range using a Perkin-Elmer Lambda 35 apparatus.

TDA-TGA analyses under H_2 were performed using a Setaram Setsys Evolution 12 thermal analyzer coupled to a Pfeiffer Omnistar mass spectrometer. Samples (30-50 mg) were placed into PtRh10% crucible before being heated from RT to 700°C (heating rate: 5°/min) under 5% H_2/Ar (flow rate: 50 cm^3/min).

Sulfided samples were characterized using Raman, X-ray photoelectron (XPS), and electron paramagnetic resonance (EPR) spectroscopies. Images of MoS_2 slabs were obtained by transmission electron microscopy.

Raman results were obtained using a LabRam HR (Horiba Jobin Yvon) spectrometer equipped with a BXFM confocal microscope, Notch filters and CCD (charge-coupled device) detector. Resolution is 1 cm^{-1}. Excitation was provided by an Ar^+-Kr^+ ion laser (514.53 nm). The laser power intensity was maintained at 100 µW to avoid any deterioration due to local heating effects during spectral acquisition.

X-ray photoelectron spectroscopy (XPS) of sulfide samples was performed using a KRATOS AXIS Ultra spectrometer. A 150 W Al Kα monochromatic source (1486.6 eV) and a hemispherical analyzer with a fixed pass energy of 40 eV were used. After sulfidation (vide infra), samples were transferred to the XPS sample holder in argon atmosphere to avoid any re-oxidation.

Binding energy values were determined considering the 74.5 eV Al 2p line as reference (accuracy: ± 0.2 eV). Mixed Gaussian and Lorentzian line shapes were used to fit curves after baseline subtraction using a Shirley-type equation (casaXPS software 2.0.71).

Mo 3d, Co 2p, and S 2p core level spectra were decomposed according to previously reported studies [39, 40]. The atomic percentage [i] of atom *i* was determined considering the respective peak area A_i and using appropriate sensitivity factors S_i:

$$[i] = \frac{\frac{A_i}{S_i}}{\sum_{i=1}^{n}(\frac{A_i}{S_i})} \qquad 1)$$

Three different contributions were considered for both Mo and Co. For molybdenum, decomposition was performed taking into account the contributions due to MoS_2 (Mo^{4+}), MoO_xS_y (Mo^{5+}) and MoO_x (Mo^{6+}) species. For cobalt, CoS_x, CoMoS (or CoO_xS_y) and CoO_x species were considered [41-45].

EPR experiments were performed on freshly sulfided samples at 77K using a Bruker ELEXSYS spectrometer (X band, 9.5 GHz). Before analysis, samples were transferred to quartz tube filled with Ar before being sealed.

TEM images were obtained using a JEOL 2100 (200 kV) microscope in order to determine MoS_2 slab length and stacking degree. Samples were ultrasonically dispersed in ethanol. The resulting suspension was then deposited onto a carbon-coated Cu grid. Average stacking number of layers per slab and average slab length were obtained as follows:

$$\overline{N} = \frac{\sum_{i=1}^{n} n_i N_i}{\sum_{i=1}^{n} n_i} \qquad 2)$$

$$\overline{L} = \frac{\sum_{i=1}^{n} n_i l_i}{\sum_{i=1}^{n} n_i} \qquad 3)$$

with N_i and l_i, the stacking number and MoS_2 slab length respectively, n being the number of particles measured in a given size range or stacking number value of index i.

2.3. Catalytic Tests

The hydrodesulfurization of 4,6-dimethyldibenzothiophene (4,6-DMDBT) was performed using a micro-pilot unit. 4,6-DMDBT was diluted into dodecane in order to reach an initial sulfur amount of 300 ppm. The 4,6-DMDBT test was carried out at 25 bars (H_2/HC (v/v) ratio of 250) at a reaction temperature of 300°C. 1.0 g of catalyst (weighted at the oxide state) was used for each test. Liquid samples were collected each hour and analyzed by gas chromatography (Agilent 6890, FID detector, CPSil-5 column: 50 m x 0.32 mm x 5 µm).

Reaction rates were determined using the following equation considering pseudo-first order rate constant:

$$v = -\frac{F_0 . d_{charge} . C_S}{m . C_0 . 32} \ln(1-\tau) \qquad 4)$$

with τ the conversion rate, m the catalyst weight (g), F_0 the molar flow of reactant (mol/h), C_0 the reactant concentration (mol/l), C_S the sulfur concentration in the feed (g/g), and d_{charge} the density of the reactant feed (g/l).

Catalyst samples were also tested in the HDS of a straight run gasoil (SRGO) feed. Initial concentration in sulfur and nitrogen were respectively 12200 ppm and 94 ppm. SRGO density was 0.837 g/cm^3. Initial and final boiling points were 167°C and 371°C. In this case, sulfidation was performed in situ using a feed comprising dimethyl disulphide (DMDS) diluted in SRGO (3.7 wt% DMDS). Experimental conditions for the sulfiding step were: P = 30 bars, LHSV = 3.0 h^{-1}, H_2/HC (v/v) ratio of 200. Temperature was maintained at 250°C for 8 h before an increase up to the final temperature of 320°C with a heating rate of 0.4°C/min.

The SRGO HDS test was performed as follows: P = 40 bars, LHSV = 2.0 h^{-1}, H_2/HC (v/v) = 300. 1.0 g of catalyst (weighted at the oxide state) was used for each test. Three different temperatures were considered: 338°C, 343°C and 348°C.

An apparent rate constant was used for determining catalytic activity [46]:

$$k_{app} = \frac{D_{vol.}}{V_{oxide}} \cdot \frac{1}{(n-1)} \cdot \left[\frac{1}{S^{(n-1)}} - \frac{1}{S_o^{(n-1)}} \right] \qquad 5)$$

with D_{vol} the volumic flow of the reactant feed (cm^3.h^{-1}), V_{oxide} the catalyst volume at the oxide state (cm^3), n = 1.2: the reaction order for the given feed used here, S_0 and S the initial and final concentration of sulfur in the feed (S_0 = 12200 ppm = 0.38125 mmol$_S$.g^{-1}).

X-ray fluorescence equipment (ANTEK-9000) was used to determine the sulfur amount of collected samples.

3. Results

3.1. Characterization of the CoMo-R Catalysts after Impregnation, Maturation and Drying Steps with EDTA, TEG and MA as Organic Additives.

3.1.1 UV-vis Analysis

The influence of the three different additives, EDTA, TEG and maleic acid (MA), was first determined after impregnation, maturation and drying. Figure 1 reports the UV-vis spectra of the regenerated $CoMo/Al_2O_3$ catalyst after addition of EDTA, TEG or MA. For comparison purposes, the UV-vis spectrum of the $CoMo/Al_2O_3$ catalyst without impregnation of additives is also presented.

CoMo-R prepared without additive presents a characteristic UV-vis spectrum with three d → d transition bands at 548, 582, and 635 nm due to Co^{2+} in interaction with the Al_2O_3 support as expected for the $CoAl_2O_4$ cobalt aluminate phase [47]. The main d → d transition band at 582 nm results from the exchange of one or several water ligands of $[Co(H_2O)_6]^{2+}$ species by Al_xOH_y (x = 1, 2, or 3; y = 0 or 1) surface ligands [47, 48].

In the case of EDTA, after impregnation, maturation and drying, the d → d transition signal shifts to lower wavelength with a main contribution now at 535 nm while the two other contributions are still observed at 580 and 635 nm. This shift to lower wavelength indicates a weaker interaction of Co species with the Al_2O_3 support which could result from a complexation of cobalt as suggested by Rinaldi et al. in the case of citric acid [28]. The interaction of Co with Al_2O_3 therefore seems to decrease after EDTA addition. Another supplementary band can also be observed at 386 nm and could correspond to a $Co^{2+} \rightarrow Co^{3+}$ transition [47]. Finally, the broad absorbance observed between 200 and 400 nm due to $O^{2-} \rightarrow Mo^{6+}$ ligand-to-metal charge transfer bands shifts to lower wavelength showing the formation of less polymerized molybdate species [49, 50].

After addition of TEG, no change in the UV-vis spectra can be discerned by comparison to the $CoMo/Al_2O_3$ catalyst prepared without additive. This shows that TEG does not interact at this stage with surface oxide species.

In the case of MA, a similar conclusion can be reached with no apparent variation in the position of the d → d transition bands after addition of maleic acid. A deeper analysis reveals anyway a small shift to lower wavelength of the d → d transition bands, from 548 to 544 nm, from 582 to 580 nm and finally from 635 to 625 nm when compared to the non-additive case. This reflects a somewhat weaker interaction of oxide species with the Al_2O_3 support. However, this effect remains marginal in comparison to the EDTA case.

3.1.2. X-ray Diffraction

The influence of the different additives was also analyzed by X-ray diffraction (Figure 2). Apart from a general pattern profile characterized by broad peaks due to γ-Al_2O_3, the regenerated alumina-supported CoMo catalyst exhibits a very clear contribution at 2θ = 26.7° due to the presence of the α-$CoMoO_4$ phase (JCPDS file # 00-021-0868). After maturation and drying with EDTA, the XRD peak due to cobalt molybdate completely disappears while weak contributions can be detected at 8.8°, 12.2°, and 17.7°. The EDTA additive very efficiently consumes Co species coming from $CoAl_2O_4$ species (Figure 1, UV-vis) or $CoMoO_4$ entities (Figure 2, XRD). Since these species correspond either to a loss of Co inside the Al_2O_3 support ($CoAl_2O_4$) or to species known to disfavor the formation of a promoted CoMoS phase after sulfidation [36], one should expect a strong beneficial effect of EDTA towards the formation of a promoted phase. Strikingly, an opposite effect is observed when using TEG since the XRD pattern is not modified after addition of triethyleneglycol. Similarly to UV-vis results, TEG seems inefficient in interacting with Co species at their oxide state. Finally, using maleic acid also leads to a complete disappearance of the α-$CoMoO_4$ XRD peak after maturation and drying. Maleic acid therefore corresponds to an intermediate situation between EDTA and TEG since it can consume efficiently Co if present in a cobalt

molybdate phase while it is unable to interact with Co if lost inside the Al_2O_3 support as $CoAl_2O_4$ entities.

In order to compare the efficiency for consuming $CoMoO_4$ when using EDTA or MA, a comparative in situ XRD study was performed during the maturation step (then before the drying step) to determine which one of the two additives is the most efficient when interacting with the cobalt molybdate phase. Note that in both cases, the maturation step was followed at 30°C and not at 90° (for EDTA) or 60°C (for MA) due to technical limitations. Note also that in the MA case, scanning was performed on a wider 2θ range to describe all the events occurring when MA is used.

In the case of EDTA (Figure 3A), maturation at 30°C does not allow consuming the $CoMoO_4$ phase characterized by a peak at 2θ = 26.7° even after 200 min showing that increasing the maturation temperature to 90°C is necessary for EDTA to consume completely cobalt aluminate species. The situation is strikingly different with MA. The $CoMoO_4$ phase starts being consumed as soon as the maturation step proceeds. After half an hour, the intensity of the XRD peak of cobalt aluminate at 2θ = 26.7°, even if still detectable, appears much weaker than initially while some intermediate XRD peaks are observed at 2θ = 26.3°, 27.8°, 28.5°, and 30.8°. After about one hour, new XRD peaks can be observed at 2θ = 24.6° and 29.9° corresponding to the (210) and (222) planes of the cobalt maleate phase, $Co(C_4H_3O_4)_2.4H_2O$ (JCPDS: 00-054-1724) [36]. This result shows that maleic acid can extract Co from the cobalt molybdate phase even after maturation at 30°C contrary to EDTA. In this way, maleic acid extracts more efficiently Co from $CoMoO_4$ than EDTA while EDTA is more efficient for extracting Co from the cobalt aluminate phase. The intermediate XRD peaks tend to disappear as cobalt maleate gradually forms. The exact nature of the intermediate phase does not correspond to any phase recorded in the JCPDS database. However, by analogy with the study made by Klimov et al. [9] about citric acid, one could expect the formation of an intermediate

mixed complex of maleic acid with Co and Mo. However, this kind of complex is stable only at a higher acidic pH (around 2.6) [51] than those observed here (3.9).

3.1.3. Thermal Analysis

Additional information about the strength of the interaction between the additive and the CoMo-R catalyst at the oxide state can be retrieved using thermogravimetric (TGA) and differential thermal (DTA) analyses. Figures 4A and B report the thermogravimetric and differential thermal analyses curves obtained respectively when submitting the CoMo-R samples prepared with EDTA, TEG, or MA to a H_2 reducing atmosphere up to 700°C. For comparison purposes, the TGA and DTA curves of CoMo-R without additive are also reported. All curves were recorded after the drying step. For the CoMo-R alone, three endothermic peaks can be noted at 86°C (water elimination), between 250°C and 350°C and around 500°C (due to dehydroxylation processes) with weight losses of 2.6% and 3.5% for the first two losses. The assignments of the TGA curves to water release or dehydroxylation processes are confirmed Figure 5A by following the mass spectrometry signal due to water formation (m/z = 18). Three peaks due to water elimination can be observed at 109°C, 246°C, and 500°C. No noticeable signal due to CO_2 (Figure 5B) can be found as expected for this catalyst prepared without organic additives.

In the case of EDTA, four better defined endothermic events can be found at 93°C, 230°C, 380°C, and 490°C with weight losses respectively of 1.3%, 2.9%, and 7.8% for the three first losses. The analysis performed by mass spectrometry (Figure 5B) shows that these endothermic events mainly correspond to water elimination around 100°C and to dehydroxylation processes. However, comparison to the mass spectrometry signal m/z = 44 due to CO_2 shows that the three latter endothermic peaks are also partly due to the elimination

of some fragments coming from the EDTA organic additive and corresponding to carboxylic groups. It should also be underlined that the onset of the CO_2 profile coincides with the decomposition temperature for EDTA (218°C).

About the impregnation with TEG, several complex endothermic events can be noted (Figure 4B). First, a peak at 80°C can be detected probably resulting from water elimination. Second, a broad signal between 195°C and 270°C can be found corresponding to several poorly defined endothermic steps. Finally, a last endothermic peak around 475°C with a shoulder at 425°C is detected. Weight losses for the first three events are respectively 1.0%, 10.5%, and 4.0% (Figure 4A). The m/z = 18 mass spectrometry signal (Figure 5A) presents a series of peaks at 98°C, 221°C, 321°C, and 458°C corresponding roughly to the endothermic events detected but with the exception of the signal around 270°C. Therefore, the peak at 98°C is due to water elimination while the other peaks are related to dehydroxylation phenomena. The m/z = 44 signal corresponds here to a CH_2-CH_2-O fragment with a main contribution at 298°C and a supplementary shoulder at 474°C. This TEG decomposition process does not occur in a simultaneous way with the loss of water suggesting a weaker interaction of TEG with the CoMo-R catalyst. The small difference in temperature between the main TEG decomposition peak on the catalyst (298°C) and the one expected for TEG alone (285°C) supports this assumption.

For maleic acid, several endothermic events are located at 95°C, 151°C, 305°C (weak), 425°C (weak), 483°C, and 588°C (Figure 4B). The absence of well-defined peaks in the TGA curve (Figure 4A) makes the determination of weight losses associated to these thermal events difficult. However, the first two events at 95°C and 151°C correspond to 6.5 wt % loss while the two endothermic peaks at 305°C and 483°C represent a 10.5 wt% loss. Peaks due to water (m/z = 18) (Figure 5A) are observed at 120°C, 175°C, and 482°C. The first two endothermic events therefore correspond respectively to water elimination and dehydroxylation. In a

similar way, the endothermic peak at 483°C is due to dehydroxylation. The m/z= 44 signal corresponds to the O-C=O fragment from maleic acid and or from its complex with Co [36] and gives rise to a broad contribution from 200°C to 500°C. This profile is due to a complex decomposition pattern characterized by a maximum at 373°C (Figure 5B) and to shoulders at 422°C and 449°C. This CO_2 formation in several steps is in agreement with the presence of two different carboxylate groups in cobalt maleate, one free carboxylic group decomposed first while the second carboxylate group interacting with cobalt is eliminated at higher temperature.

The maximum for MA decomposition is observed at a temperature (373°C) much higher than the decomposition temperature for free maleic acid (135°C) showing a very strong interaction of this organic additive with CoMo-R. Comparison between decomposition temperatures on CoMo-R and for the three free organic additives is provided in Table 1. The difference in temperature between impregnated and free additives is the highest for MA (ΔT = 238°C) followed by EDTA (ΔT = 163°C) while only a small difference of only 13°C is found for TEG. In this respect, the TGA-DTA study coupled to mass spectrometry analysis shows that maleic acid is the organic additive interacting the most strongly with the regenerated $CoMo/Al_2O_3$ catalyst. This result is in agreement with the previous XRD analysis showing the high efficiency of maleic acid to interact with Co if present in cobalt molybdate species.

3.2. HDS Catalytic Properties

Results acquired previously during the impregnation step of regenerated $CoMo/Al_2O_3$ with different additives have underlined strong differences among the three organic compounds considered here. The TEG additive only presents a very weak interaction with the CoMo-R catalyst as confirmed by TGA-DTA analysis and appears unable to extract Co species

whatever their nature (cobalt aluminate or cobalt molybdate). On the contrary, EDTA is able to extract Co coming either from $CoAl_2O_4$ or from $CoMoO_4$ entities. Finally, MA presents a contrasting behavior: while it is unable to extract Co from cobalt aluminate, MA consumes cobalt from cobalt molybdate in a more efficient way than EDTA. This last point is particularly interesting since the oxidative regeneration procedure should favor the formation of cobalt molybdate species. Moreover, among the three organic additives, MA is the one interacting the most with the regenerated $CoMo/Al_2O_3$ catalyst. Therefore, it is interesting to determine how these different comportments can influence the HDS catalytic properties of the regenerated $CoMo/Al_2O_3$ catalyst after its impregnation with the different additives.

3.2.1. Hydrodesulfurization of 4,6-Dimethyldibenzothiophene

The catalytic activity was first evaluated for the hydrodesulfurization of a model compound, 4,6-dimethyldibenzothiophene (4,6-DMDBT) representative of refractory-to-be desulfurized molecules. Table 2 reports the catalytic activity results after 4,6-DMDBT HDS test at 300°C following an ex situ sulfidation at 350°C. First of all, previous results [36] have shown that the regenerating step without using organic additives allows to retrieve only 85% of the initial activity found using the equivalent fresh catalyst. After addition of organic additives, the HDS activity increases significantly whatever the nature of the additive used. However, EDTA and MA are the most efficient additives in terms of HDS activity improvement with respectively reaction rates 96% and 83% higher than for the CoMo-R sample prepared without additive. The TEG additive leads to a more moderate increase with a reaction rate 43% higher than for CoMo-R alone. Selectivity results are also reported in Figure 6. Only the two main products of the HDS of 4,6-DMDBT along the two parallel pathways are detected: 3,3'-dimethylbiphenyl (3,3'-DMBP) along the so-called direct desulfurization route (DDS) and

dimethylcyclohexylbenzene (DMCHB) along the hydrogenating route. Neither the partially hydrogenated but still sulfurized hexahydrodimethyldibenzothiophene compound nor the completely hydrogenated and desulfurized dimethylbicyclohexyl are observed. Addition of the TEG additive does not modify selectivity properties by comparison to the CoMo-R catalyst prepared without additive with a selectivity along the DDS pathway of 52%. This suggests that TEG does not influence the nature of the active phase formed during sulfidation and HDS test. On the opposite, using EDTA or MA favors the formation of 3,3'-DMBP along the DDS pathway (selectivities of 58% and 61% using EDTA and MA respectively). It is well known that promotion by cobalt induces a higher selectivity along the DDS route [52-55]. This result might indicate in this case that a better decoration of MoS_2 particles by the cobalt promoter was achieved using either EDTA or MA.

3.2.2. Hydrodesulfurization of a Straight Run Gasoil (SRGO) Feed

In order to differentiate more clearly the efficiency of the different organic additives, the same CoMo-R samples prepared with TEG, EDTA, or MA were also tested in a more demanding HDS reaction using a straight-run gas oil (SRGO) feed. Table 3 reports the results obtained at three different temperatures of reaction (338°C, 343°C, and 348°C). Rate constant values and residual S amounts are indicated in each case. The first point to note is that under these harsher conditions, the previously moderate beneficial effect of TEG is not observed anymore with residual S amounts slightly higher at the three different temperatures of reaction than for the CoMo-R sample prepared without additive. Note that TEG can present slightly higher rate constant values at 338°C and 343°C than without additive but also at the same time higher residual S amounts since rate constant values have to be corrected to take into account the increase of the catalyst mass resulting from the organic additive addition. However, even in

this case, the rate constant of the CoMo-R sample prepared with TEG becomes lower than without additive at a temperature of reaction of 348°C (15.8 vs 16.4 $g^{0.2}.mmol^{-0.2}.h^{-1}$). On the opposite, EDTA or MA still presents a strong beneficial effect whatever the temperature of reaction. However, under SRGO HDS conditions, differences can be observed between EDTA and MA, MA being this time much more active than EDTA. In this respect, at a temperature of reaction of 348°C, the rate constant achieved by the CoMo-R sample prepared with MA is 73% higher than without additive and 45% higher than with EDTA. This results in a residual S amount of 52 ppm with MA vs 172 ppm with EDTA showing a clear stronger beneficial effect of MA in the present case.

The present results therefore emphasize the marked superiority of maleic acid as an additive compared to EDTA or TEG during the impregnation of regenerated alumina-based CoMo catalysts leading to a strong enhancement of HDS catalytic properties particularly when devoted to the removal of refractory sulfur-containing molecules present in real feedstocks. This situation is quite significant if direct comparison is made between EDTA and MA and can be related to a more efficient extraction of cobalt from cobalt molybdate species when using maleic acid. It is interesting to note that, contrary to MA, EDTA is able to extract Co from $CoAl_2O_4$ entities without any significant effect on the final HDS activity suggesting that when extracted from cobalt aluminate, Co cannot be dispersed efficiently on MoS_2 particles after sulfidation. This reflects the necessity to better analyze the activation process of regenerated $CoMo/Al_2O_3$ prepared with MA.

3.3. Activation of Regenerated $CoMo/Al_2O_3$ in the Presence of Maleic Acid

3.3.1. Elemental Analysis

To ascertain the kinetics of sulfidation of CoMo-R in the presence or not of maleic acid, S and C elemental amounts were first determined at several temperatures of sulfidation: RT, 150°C, 250°C, 300°C, and finally the final sulfidation temperature of 350°C. Since results were already reported previously [36], only a brief summary of the results will be displayed here (Supporting Information, Table S1). At RT, similar S/(Co+Mo) atomic ratios were found whether MA was used or not. However, at a temperature of sulfidation of 150°C, addition of MA results in a much higher sulfidation rate with a S/(Co+Mo) ratio of 1.95 vs 1.53 in the absence of MA. As soon as the temperature of sulfidation reaches 250°C, both samples are already sulfided in a large extent and only a very moderate increase of the S/(Co+Mo) ratio is observed above the 250°C threshold. Both catalysts then present similar S/(Co+Mo) ratios after being sulfided at 300°C.

3.3.2 Mass Spectrometry Analysis

In order to clarify the nature of the species formed during the activation of CoMo-R impregnated with MA, mass spectrometry analysis was performed during the sulfidation stage. Three main species are observed: CO_2, cyclopropane, and propane. Minor amounts of butane and COS are also formed. The CO_2 signal presents a main contribution at 313°C with a shoulder around 210°C showing that the MA additive does not decompose in a large extent before 300°C [36]. Similarly, cyclopropane and propane show main contribution peaks in a similar temperature range: 310°C for cyclopropane and 328°C for propane (Supplementary Information, Figure S2). Therefore, the main sulfur uptake during the activation step is observed around 150°C while sulfidation is performed in a large extent as soon as 250°C. However, this sulfidation occurs before the MA decomposition showing that the additive is still complexed to Co even during the activation.

3.3.3. X-ray Photoelectron Spectroscopy Analysis

Determination of the different species formed during the activation was also performed using X-ray photoelectron spectroscopy. Detailed results have already been presented previously [36] and only a summary of the main results will be given below. Mo 3d XPS core-level spectra are generally decomposed into three main contributions corresponding to the different degrees of oxidation: +VI (oxide), +V (oxysulfide) and +IV (sulfide) [41-43]. Co 2p XPS core-level spectra are also decomposed into three contributions corresponding to CoO_x oxide species, non-promoted CoS_x sulfide species and finally a contribution with intermediate binding energy range between oxides and sulfides corresponding either to cobalt oxysulfide at low temperatures of sulfidation or to the promoted CoMoS phase at high temperatures of sulfidation. Note that distinguishing these two latter species is not possible since only a slight binding energy difference (≤ 0.4 eV) exists between them. Table S2 summarizes the proportion of each Mo and Co species at a given temperature of sulfidation. About Mo 3d XPS species, at $T°_{sulf}$ = 150°C, the addition of maleic acid induces a decrease of the proportion of Mo^{6+} oxide species (from 51% to 28%) in agreement with elemental analysis results. However, this higher sulfidation degree results from a higher proportion of Mo^{5+} oxysulfide species using MA (29% vs 6%) and not from any difference in the amount of fully sulfided Mo^{4+} species. This result was previously ascribed to a higher redispersion of Mo species as $AlMo_6$ Anderson entities when using MA. Above $T°_{sulf}$ = 250°C, no significant difference in the sulfidation degree can be observed whether MA was used or not.

About the Co 2p XPS spectra, sulfidation already partly occurs at RT. However, in the presence of MA, this leads to a higher percentage of Co oxysulfide species showing that in the presence of the additive, Co starts being sulfided while still linked to some oxygen ligands

coming from maleate groups. A similar situation is still observed after sulfidation at 150°C with 54% of cobalt oxysulfide species if MA is present vs 36% in its absence. This situation is progressively reversed at $T°_{sulf} \geq 250°C$ with more or less similar proportions in Co species whatever the presence or the absence of MA. Interestingly, after sulfidation at the final temperature of 350°C, the use of MA as additive results in a higher proportion of promoted CoMoS phase (82 % vs 74%). This can be related to a faster sulfidation of molybdenum in the presence of MA while Co is kept inside a maleate complex even if partially sulfided. After decomposition of the complex, this leads to a better availability of Co for decorating MoS_2 layers without forming a non-promoted CoS_x phase.

3.3.4. Electron Paramagnetic Resonance Spectroscopy

Additionally, CoMo-R was also characterized during sulfidation using EPR spectroscopy since this technique is sensitive to the presence of paramagnetic Mo^{5+} entities. Four main signals can be detected at g = 1.904 (Mo^{5+} -oxo or oxysulfide), 1.950 (carboxylate radical species), 1.978 (C sp^2 radical organic species), and $g_{\perp} = 2.009$, $g_{//} = 2.030$ (thio-Mo^{5+}) [56, 57]. Figure 7 reports the EPR spectra of CoMo-R prepared or not in the presence of MA at the different temperatures of sulfidation (RT, 150°C, 250°C, 300°C). The signal at g = 1.904 due to Mo^{5+} -oxo or oxysulfide species varies in a large extent with the temperature of sulfidation particularly for the CoMo-R sample prepared with MA. Figure S3 reports the relative variation of the amount of Mo^{5+} -oxo or oxysulfide species at the different temperatures of sulfidation in the presence or not of the MA additive. Results show that whatever the temperature of sulfidation, a higher proportion of Mo^{5+} -oxo or oxysulfide species are found in the absence of MA. In this case, the amount of Mo^{5+} -oxo or oxysulfide species increases up to $T°_{sulf}$ = 150°C before stabilization. In the presence of MA, a more marked increase is

observed up to 250°C, temperature at which MA starts decomposing while at $T°_{sulf}$ > 250°C, a decrease is observed. Previous XPS results (see Table S2) showed a higher amount of Mo^{5+} oxysulfide species in the presence of MA at least up to $T°_{sulf}$ = 250°C. Moreover, EPR cannot distinguish between Mo^{5+} species not or partly sulfided. Therefore, the present results show that MA favors the formation of Mo^{5+} oxysulfides while sulfidation performed without MA leads to a predominance of non-sulfided Mo^{5+} -oxo species.

3.3.5. Raman Spectroscopy Analysis

The sulfidation procedure of the regenerated $CoMo/Al_2O_3$ catalyst in the presence or not of MA was also followed by Raman spectroscopy. Figures 8A and 8B reports the evolution of the Raman spectra in the 150-600 cm^{-1} range for different temperatures of sulfidation (150°C, 250°C, 300°C, 350°C) in the absence or presence of MA respectively.

In the absence of MA, sulfidation at 150°C does not lead to any clear contributions suggesting that molybdenum was not sulfided yet. At 250°C, two broad bands can be detected around 300-350 cm^{-1} and around 400-410 cm^{-1}. The 300-350 cm^{-1} signal is attributed to molybdenum sulfide still presenting mainly an amorphous character [58, 59] while the weak signal at 400-410 cm^{-1} is due to the ν(Mo-S) (E // c) vibration band perpendicular to the basal plane of MoS_2 [60-69]. This latter band increases in intensity after sulfidation at 300°C while a new band can now be detected at 374 cm^{-1}. This new signal is related to the ν(Mo-S) (E ⊥ c) vibration along the MoS_2 basal plane. After sulfidation at 350°C, the bands at 374 and 409 cm^{-1} still increase but in a minor extent. These results are in agreement with those obtained by decomposing Mo 3d XPS core level spectra showing that sulfidation of molybdenum becomes really significant around 250°C and continues in a progressive way up to 350°C.

In the case of the addition of MA for activating CoMo-R, marked differences can be noted on the Raman spectra acquired at the different temperatures of sulfidation. First, after sulfidation at 150°C, a higher sulfidation advancement can be noted characterized by the appearance of two clear bands at 320 and 442 cm^{-1}. This latter band can be attributed to a ν(Mo-S-Mo) elongation vibration mode of molybdenum oxysulfide species [58, 60]. This result is in agreement with both elemental analysis and XPS results. This higher sulfidation degree of the CoMo-R catalysts in the presence of MA at 150°C therefore results from a higher amount of oxysulfide species formed when using MA. After sulfidation at 250°C, the Raman spectrum does not present anymore any contribution particularly at 442 cm^{-1} showing the disappearance of clearly organized oxysulfide species and the formation of a molybdenum sulfide phase still largely amorphous. At $T°_{sulf}$ = 300°C, two new ν(Mo-S) bands become detectable at 374 and 409 cm^{-1} showing the formation of the MoS_2 phase. Finally, sulfiding at 350°C leads to a significant increase of the intensity of these two bands in agreement with the higher proportion of Mo^{4+} species detected by XPS (Table S2). Interestingly, by comparison to the preceding case without MA, a lower relative I(409)/I(374) intensity ratio can be observed using MA. This suggests a higher structural disorder along the c stacking direction for the MoS_2 slabs. This would be related to the presence of residual carbon coming from the MA additive known to favor the formation of stacking faults [70-72].

3.3.6. Transmission Electron Microscopy

TEM characterization was also performed after sulfidation at 150°C, 250°C, 300°C, and 350°C for both cases, without or with MA. Corresponding TEM images are reported in Figure S4, Supplementary Information. Sulfidation at 150°C does not lead to the formation of any fringes characteristic of MoS_2 slabs if activation is performed without MA. Using the MA

additive leads to the presence of few MoS_2 fringes confirming a higher sulfidation advancement in this case (Figure S4B). Sulfiding at 250°C results in the detection of MoS_2 fringes in both cases, with or without MA added during the CoMo-R preparation. However, sulfidation at 300°C and 350°C emphasizes a higher structural disorder of the stacking of the MoS_2 slabs if MA is used in agreement with the previous observations made by Raman spectroscopy. Statistical results about average MoS_2 slab length and stacking degree have been obtained after sulfidation at 250°C, 300°C and 350°C (Table 4). Note that the low amount of MoS_2 particles detected after sulfidation at 150°C in the presence of MA does not allow to retrieve a meaningful statistical result. As soon as $T°_{sulf}$ = 250°C, average slab length and stacking degree remain constant whatever the sulfidation temperature showing that the final morphology of the MoS_2 particles is already reached after sulfidation at 250°C. Moreover, there is no difference in terms of average slab length or stacking degree when comparing results acquired with or without MA. Therefore, using the MA additive does not influence the dispersion of the MoS_2 phase even if a more disordered stacking can be detected if MA is used. Knowing the average slab length and the 4,6-DMDBT HDS activity measured previously, it was possible using a geometrical model for MoS_2 slabs to evaluate the turnover frequency (TOF) of each sample (with or without MA) considering Mo atoms on edge MoS_2 planes as the active sites for the HDS reaction [36]. Results showed TOF values respectively of 0.65 h^{-1} for CoMo-T without MA and 1.37 h^{-1} with MA. Taking into account the respective proportion of CoMoS phase for each sample (58% for CoMo-R, 68% for CoMo-R/MA), the gain in TOF observed cannot result from a higher amount of CoMoS sites with similar intrinsic activity in both cases. In fact, a rough calculation suggests that CoMoS sites obtained in the presence of MA are about 80% more intrinsically active for the HDS of 4,6-DMDBT than CoMoS sites obtained without additive.

4. Discussion

The whole results acquired in the present study and in our previous work [36] allows proposing a general description of the sulfidation mechanism of the regenerated $CoMo/Al_2O_3$ catalyst prepared with the maleic acid additive. First of all, it seems important to consider the sulfidation of the complex formed between cobalt and maleic acid by itself. Results showed that cobalt maleate can in fact be sulfided before its degradation around 310°C into CO_2 and various hydrocarbons (mainly propane and cyclopropane, see Figure S2). Indeed, sulfidation at low temperature leads to the formation of CoO_xS_y entities corresponding to Co-S moieties still linked to carboxylate ligands.

The initial structure of cobalt maleate, $Co(C_4H_3O_4)_2.4H_2O$ comprises four water ligands. However, these ligands are not equivalent in a structural point of view. Two of them present a higher stabilization resulting from the presence of hydrogen bonding with the neighboring carboxyl groups of the maleate ligand. Sulfidation would then start at low temperature through the replacement of the two non-stabilized water ligands forming S_2^{2-} groups linked to a cobalt atom still bonded to carboxylate ligands. These S_2^{2-} groups would then be transformed into S^{2-} entities at a higher temperature of sulfidation. The next step corresponds to a purely thermal decomposition process of cobalt maleate, identical to what was observed previously on acrylate compounds and corresponding to a dehydration step below 200°C [73, 74].

The removal of the two last water ligands by dehydration leads to a structure similar to the $[CoC_4H_2O_4.2H_2O]_n$ fragment resulting from the dehydration of the $CoC_4H_2O_4.4H_2O$ cobalt maleate compound [75, 76]. Inside this compound, cobalt presents a +II oxidation degree and is linked to four oxygen atoms forming a tetradentate compound. Above 250°C, this structure starts decomposing with H_2 consumption forming CO_2 and various hydrocarbon compounds.

Moreover, the simultaneous elimination of the hydrocarbons at a temperature similar to the one observed for CO_2 suggests that the olefinic bonds are probably hydrogenated at least partly before decomposition of the ligand coordinated to cobalt. A general description of the whole process is provided Figure 9.

If we now consider the mechanism of sulfidation of the regenerated catalyst prepared with maleic acid, five different steps can be distinguished. During the impregnation step, maleic acid interacts selectively with the $CoMoO_4$ phase while $CoAl_2O_4$ remains untouched by the additive (Figure 10). This selective interaction with $CoMoO_4$ leads to the formation of cobalt maleate and to a redispersion of Mo species as $AlMo_6$ Anderson salts. Sulfidation at low temperature then leads to a high sulfur consumption particularly around 150°C leading 1) to a partial sulfidation of cobalt maleate still linked to carboxylate ligands and 2) to a rapid sulfidation of well-dispersed $AlMo_6$ species producing mainly molybdenum oxysulfides. As shown above, this low temperature sulfidation step is accompanied by a dehydration of cobalt maleate leading to tetradentate cobalt sulfide entities. After sulfidation at 300°C, the partially sulfided cobalt maleate is decomposed forming CO_2 and hydrocarbons. The as-formed cobalt oxysulfide species are then rapidly sulfided into cobalt sulfide entities able to interact with the already formed molybdenum sulfide particles. After sulfidation at 350°C, the complete decomposition of cobalt maleate allows the promoter to efficiently interact with the edge sites of MoS_2 slabs enhancing the formation of the promoted CoMoS phase.

Conclusion

The exact role of maleic acid as organic additive improving the activity of regenerated $CoMo/Al_2O_3$ HDS catalyst has been herein clarified by comparison to two other commonly used additives, a chelating agent, ethylenediaminetetraacetic acid (EDTA) and a glycol-type compound, triethyleneglycol (TEG) after impregnation and drying steps. Quite different

behavior was noticed when comparing maleic acid to EDTA or TEG. First of all, TEG was found inefficient towards cobalt extraction from either $CoMoO_4$ or $CoAl_2O_4$. Maleic acid was able to extract only cobalt from $CoMoO_4$ species while EDTA can be used to recover cobalt from both $CoMoO_4$ and $CoAl_2O_4$. However, in situ XRD reveals that maleic acid is also more efficient in extracting cobalt from cobalt molybdate than EDTA. This was confirmed by TGA-DTA analysis. Evaluation of HDS catalytic properties showed that maleic acid is the most efficient in restoring the activity of the regenerated $CoMo/Al_2O_3$ particularly when HDS tests are performed on real feedstock.

Finally, the activation process of the regenerated $CoMo/Al_2O_3$ catalyst in the presence of maleic acid was carefully studied showing partial sulfidation of the cobalt maleate complex before its decomposition allowing an optimal distribution of the cobalt promoter onto already well-dispersed MoS_2 particles.

Acknowledgment

N.-Q. Bui thanks region Rhône-Alpes for financial support.

References

[1] G. Berhault, Metal Sulfides: Novel Synthesis Methods and Recent Developments, in: V. Parvulescu, E. Kemnitz, (Eds.), New Materials for Catalytic Applications, Elsevier, 2016, pp. 313-360.

[2] A. López-Benítez, G. Berhault, A. Guevara-Lara, Appl. Catal. B: Environmental, 213 (2017) 28-41.

[3] A. López-Benítez, G. Berhault, L. Burel, A. Guevara-Lara, J. Catal. 354 (2017) 197-212.

[4] T.S. Nguyen, S. Loridant, C. Lorentz, T. Cholley, C. Geantet, Appl. Catal. B: Environmental 107 (2011) 59-67.

[5] M.A. Lélias, E. Le Guludec, L. Mariey, J. van Gestel, A. Travert, L. Oliviero, F. Maugé, Catal. Today 150 (2010) 179-185.

[6] S. Badoga, K. Chandra Mouli, K.K. Soni, A.K. Dalai, J. Adjaye, Appl. Catal. B: Environmental 125 (2012) 67-84.

[7] T. Kubota, N. Rinaldi, K. Okumura, T. Honma, S. Hirayama, Y Okamoto, Appl. Catal. A: General 373 (2010) 214-221.

[8] S.I. Lee, A. Cho, J.H. Koh, S.H. Oh, S.H. Moon, Appl. Catal. B: Environmental 101 (2011) 220-225.

[9] O.V. Klimov, A.V. Pashigreva, M.A. Fedotov, D.I. Kochubey, Y.A. Chesalov, G.A. Bukhtiyarova, A.S. Noskov, J. Mol. Catal. A 322 (2010) 80-89.

[10] S. Badoga, A.K. Dalai, J. Adjaye, Y. Hu, Ind. Eng. Chem. Res. 53 (2014) 2137−2156.

[11] P. Castillo-Villalón, J. Ramirez, J.A. Vargas-Luciano, J. Catal. 320 (2014) 127-136.

[12] A. Pimerzin, A. Mozhaev, A. Varakin, K. Maslakov, P. Nikulshin, Appl. Catal. B: Environmental 205 (2017) 93-103.

[13] V. Costa, K. Marchand, M. Digne, C. Geantet, Catal. Today 130 (2008) 69–74.

[14] D. Nicosia, R. Prins, J. Catal. 234 (2005) 414-420.

[15] T.S. Nguyen, S. Loridant, C. Lorentz, T. Cholley, C. Geantet, Appl. Catal. B 107 (2011) 59– 67.

[16] A. Gutierrez-Alejandre, G. Laurrabaquio-Rosas, J. Ramirez, G. Busca, Appl. Catal. B 166 (2015) 560-567.

[17] L. Coulier, V.H.J. de Beer, J.A.R. van Veen, J.W. Niemantsverdriet, J. Catal. 197 (2001) 26-33.

[18] A.M. de Jong, V.H.J. de Beer, J.A.R. van Veen, J.W. Niemantsverdriet, J. Phys. Chem. 100 (1996) 17722-17724.

[19] G. Kishan, L. Coulier, V.H.J. de Beer, J.A.R. van Veen, J.W. Niemantsverdriet, J. Catal. 196 (2000) 180-189.

[20] G. Kishan, L. Coulier, V.H.J. de Beer, J.A.R. van Veen, J.W. Niemantsverdriet, Chem. Comm. (2000) 1103-1104.

[21] G. Kishan, L. Coulier, J.A.R. van Veen, J.W. Niemantsverdriet, J. Catal. 200 (2001) 194-196.

[22] L. Medici, R. Prins, J. Catal. 163 (1996) 38-49.

[23] R. Cattaneo, T. Shido, R. Prins, J. Catal. 185 (1999) 199-212.

[24] P. Mazoyer, C. Geantet, F. Diehl, S. Loridant, M. Lacroix, Catal. Today 130 (2008) 75-79.

[25] L. van Haandel, G.M. Bremmer, E.J.M. Hensen, Th. Weber, J. Catal. 351 (2017) 95-106.

[26] Y. Yoshimura, N. Matsubayashi, T. Sato, H. Shimada, A. Nishijima, Appl. Catal. A 79 (1991) 145-159.

[27] T. Fujikawa, H. Kimura, K. Kiriyama, K. Hagiwara, Catal. Today 111 (2006) 188-193.

[28] N. Rinaldi, Usman, K. Al-Dalama, T. Kubota, Y. Okamoto, Appl. Catal. A 360 (2009) 130-136.

[29] N. Rinaldi, T. Kubota, Y. Okamoto, Appl. Catal. A 374 (2010) 228-236..

[30] O.V. Klimov, A.V. Pashigreva, M.A. Fedotov, D.I. Kochubey, Y.A. Chesalov, G.A. Bukhtiyarova, A.S. Noskov, J. Mol. Catal. A 322 (2010) 80-89.

[31] A.V. Pashigreva, G.A. Bukhtiyarova, O.V. Klimov, Y.A. Chesalov, G. Litvak, A.S. Noskov, Catal. Today 149 (2010) 19-27.

[32] J.J. Chen, J.X. Mi, K.Z. Li, X.Q. Wang, E.D. Garcia, Y.N. Cao, L.L. Jiang, L. Oliviero, F. Maugé, Ind. Eng. Chem. Res. 56 (2017) 14172-14181.

[33] P. Afanasiev, Appl. Catal. A 529 (2017) 10-19.

[34] P. Dufresne, N. Brahma, F. Girardier, Rev. Inst. Fr. Petrol. 50 (1995) 283-293.

[35] V. Teixeira Da Silva, R. Frety, M. Schmal, Ind. Eng. Chem. Res. 33 (1994) 1692-1699.

[36] N.-Q. Bui, C. Geantet, G. Berhault, J. Catal. 330 (2015) 374–386.

[37] S.V. Budukva, O.V. Klimov, Y.A. Chesalov, I.P. Prosvirin, T.V. Larina, A.S. Noskov, Catal. Lett. 148 (2018) 1525-1534.

[38] J.R. Allan, G.M. Baillie, J.G. Bonner, D.L. Gerrard, S. Hoey, Thermochimica Acta 143 (1989) 283-288.

[39] D. Laurenti, B. Phung-Ngoc, C. Roukoss, E. Devers, K. Marchand, L. Massin, L. Lemaitre, C. Legens, A.A. Quoineaud, M. Vrinat, J. Catal. 297 (2013) 165–175.

[40] A.D. Gandubert, E. Krebs, C. Legens, D. Costa, D. Guillaume, P. Raybaud, Catal. Today 130 (2008) 149-159.

[41] A. Galtayries, S. Wisniewski, J. Grimblot, J. Electron Spectros. Related Phenomena 87 (1997) 31-44.

[42] A.M. Venezia, Catal. Today 77 (2003) 359-370.

[43] J.C. Dupin, D. Gonbeau, I. Martin-Litas, Ph. Vinatier, A. Levasseur, Appl. Surf. Sci. 173 (2001) 140-150.

[44] L. Coulier, V.H.J. de Beer, J.A.R. van Veen, J.W. Niemantsverdriet, Top. Catal. 13 (2000) 99-108.

[45] Th. Weber, J.C. Muijsers, J.W. Niemantsverdriet, J. Phys. Chem. 99 (1995) 9194-9200.

[46] D. Letourneur, R. Bacaud, M. Vrinat, D. Schweich, I. Pitault, Ind. Eng. Chem. Res. 37 (1998) 2662-2667.

[47] J. H. Ashley, P. C. H. Mitchell, J. Chem. Soc. A 90 (1968) 2821-2827

[48] J. Vakros, K. Bourikas, S. Perlepes, C. Kordulis, A. Lycourghiotis, Langmuir 20 (2004) 10542-10550.

[49] M. Fournier, C. Louis, M. Che, P. Chaquin, D. Masure, J. Catal. 119 (1989) 400-414.

[50] R.S. Weber, J. Catal. 151 (1995) 470-474.

[51] S.L. González-Cortés, Y. Qian, H.A. Almegren, T. Xiao, V.L. Kuznetsov, P.P. Edwards, Appl. Petrochem. Res. 5 (2015) 181-197.

[52] F. Bataille, J.L. Lemberton, P. Michaud, G. Pérot, M. Vrinat, M. Lemaire, E. Schulz, M. Breysse, S. Kasztelan, J. Catal. 191 (2000) 409-422.

[53] T. Kabe, A. Ishihara, Q. Zhang, Appl. Catal. A 97 (1993) L1-L9.

[54] V. Meille, E. Schulz, M. Lemaire, M. Vrinat, J. Catal. 170 (1997) 29-36.

[55] G. Berhault, M. Perez de la Rosa, A. Mehta, M. José-Yacaman, R.R. Chianelli, Appl. Catal. A 345 (2008) 80-88.

[56] B.G. Silbernagel, T.A. Pecoraro, R.R. Chianelli, J. Catal. 78 (1982) 380-388.

[57] A.J.A. Konings, A.M. van Dooren, D.C. Koningsberger, V.H.J. De Beer, A.L. Farragher, G.C.A. Schuit, J. Catal. 54 (1978) 1-12.

[58] E. Payen, S. Kasztelan, S. Houssenbay, R. Szymanski, J. Grimblot, J. Phys. Chem. 93 (1989) 6501-6506.

[59] G.L. Schrader, C.P. Cheng, J. Catal. 85 (1984) 488-498.

[60] G.L. Schrader, C.P. Cheng, J. Catal. 80 (1983) 369.

[61] E. Payen, S. Kasztelan, J. Grimblot, J. Mol. Struct. 174 (1988) 71

[62] F.R. Brown, L.E. Makovsky, K.H. Rhee, J. Catal. 50 (1977) 385.

[63] E. Payen, M.C. Dhamelincourt, P. Dhamelincourt, J. Grimblot, J.P. Bonnelle, Appl. Spectrosc. 36 (1982) 30.

[64] A. Müller, T. Weber, Appl. Catal. 77 (1991) 243.

[65] H.J. Conley, B. Wang, J.I. Ziegler, R.F. Haglund, S.T. Pantelides, K.I. Bolotin, Nano Lett. 13 (2013) 3626-3630.

[66] S. Sahoo, A.P.S. Gaur, M. Ahmadi, M.J.F. Guinel, R.S. Katiyar, J. Phys. Chem. C 117 (2013) 9042-9047

[67] S. Mukherjee, S. Biswas, A. Ghorai, A. Midya, S. Das, S.K. Ray, J. Phys. Chem. C 122 (2018) 12502-12511.

[68] C. Zhang, L. Jiang, Y. Zhang, J. Hu, M.K.H. Leung, J. Catal. 361 (2018) 384-392.

[69] E. Blanco, P. Afanasiev, G. Berhault, D. Uzio, S. Loridant, C.R. Chim. 19 (2016) 1310-1314.

[70] G. Berhault, A. Mehta, A. Pavel, J. Yang, L. Rendon, M.J. Yacamán, L. Cota, A. Duarte, R.R. Chianelli, J. Catal. 198 (2001) 9-19.

[71] G. Berhault, L. Cota Araiza, A. Duarte Moller, A. Mehta, R. R. Chianelli, Catal. Lett. 78 (2002) 81-90.

[72] G. Alonso, G. Berhault, A. Aguilar, V. Collins, C. Ornelas, S. Fuentes, R. R. Chianelli, J. Catal. 208 (2002) 359-369.

[73] E.I. Aleksandrova, G.I. Dzhardimalieva, A.S. Rosenberg, A.D. Pomogailo, Russ. Chem. Bull. 42 (1993) 259-263.

[74] A.S. Rosenberg, E.I. Aleksandrova, G.I. Dzhardimalieva, N.V. Kiryakov, P.E. Chizhov, V.I. Petinov, A.D. Pomogailo, Russ. Chem. Bull. 44 (1995) 858-866.

[75] A.S. Rosenberg, E.I. Aleksandrova, N.P. Ivleva, G.I. Dzhardimalieva, A.V. Raevskii, O.I. Kolesova, I.E. Uflyand, A.D. Pomogailo, Russ. Chem. Bull. 47 (1998) 259-264.

[76] N.P. Porollo, Z.G. Aliev, G.I. Dzhardimalieva, I.N. Ivleva, I.E. Uflyand, A.D. Pomogailo, N.S. Ovanesyan, Russ. Chem. Bull. 46 (1997) 362-370.

Figure Captions

Figure 1: UV-vis spectra of the regenerated CoMo-R catalyst prepared with EDTA, TEG, or MA. Results are provided after impregnation, maturation and drying onto CoMo-R. For comparison purposes, the UV-vis spectrum of CoMo-R without additive is also presented.

Figure 2: X-ray diffraction patterns of the regenerated CoMo-R catalyst prepared with EDTA, TEG, or MA. Results are provided after impregnation, maturation and drying onto CoMo-R. For comparison purposes, the XRD pattern of CoMo-R without additive is also presented.

Figure 3: Evolution of the XRD patterns of the CoMo-R catalyst in function of the time of maturation after addition of A) EDTA or B) MA.

Figure 4: Evolution of TGA (A) and DTA (B) curves of the CoMo-R catalyst prepared with EDTA, TEG, or MA under 5% H_2/Ar atmosphere (heating rate: 5°/min, flow rate: 50 cm^3/min). For comparison purposes, the TGA and DTA curves of the CoMo-R catalysts prepared without additive are also presented.

Figure 5: Evolution of the mass spectrometry signals corresponding to m/z = 18 (A) or m/z = 44 (B) when submitting CoMo-R prepared with EDTA, TEG, or MA to a reducing treatment under 5% H_2/Ar atmosphere (heating rate: 5°/min, flow rate: 50 cm^3/min). For comparison purposes, the same m/z = 18 or 44 signals were also recorded for the CoMo-R sample prepared without additive.

Figure 6: Selectivity in the HDS of 4,6-dimethyldibenzothiophene for the CoMo-R samples prepared with TEG, EDTA, or MA. Results are also provided in the absence of additive. Values are given at a conversion of 20%.

Figure 7: EPR spectra of the CoMo-R catalyst prepared or not in the presence of maleic acid and sulfided at RT, 150°C, 250°C, and finally 300°C.

Figure 8: Raman spectra of the CoMo-R catalyst prepared without (A) or with (B) maleic acid and sulfided at different temperatures of sulfidation.

Figure 9: Reaction scheme describing the cobalt maleate sulfidation process.

Figure 10: General description of the activation mode of maleic acid for restoring the HDS activity of the CoMo-R catalyst.

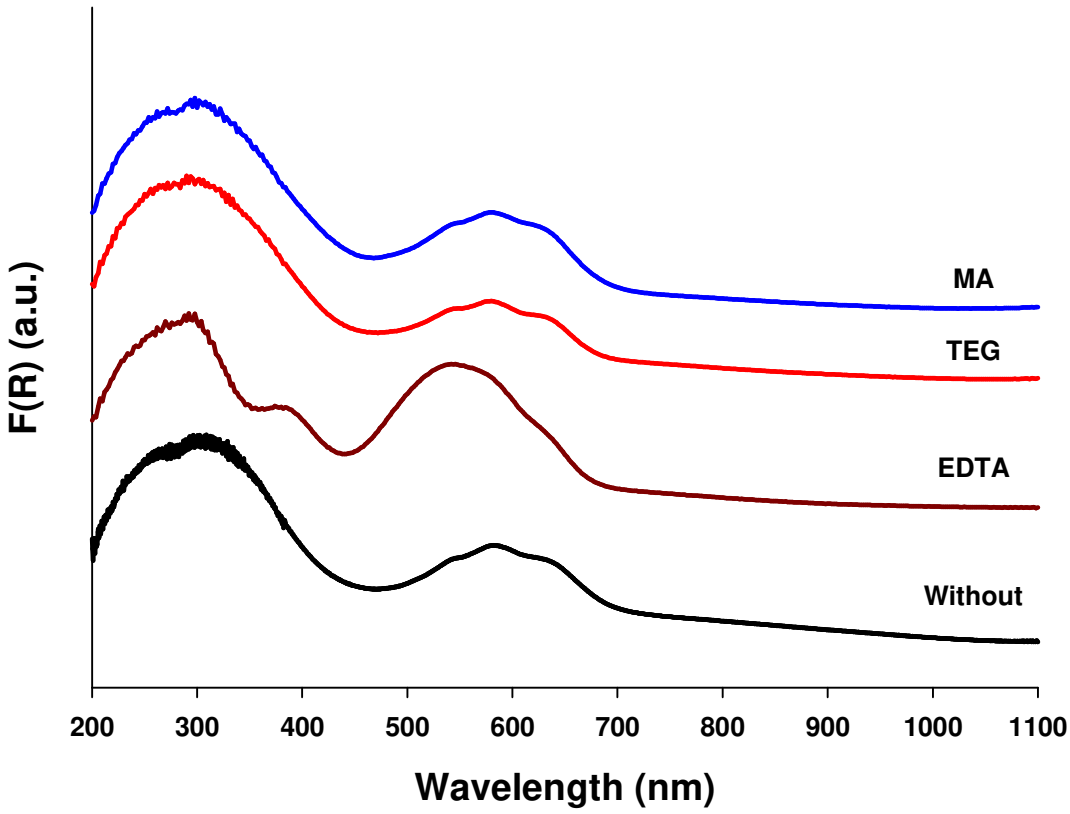

Bui et al.

Figure 1

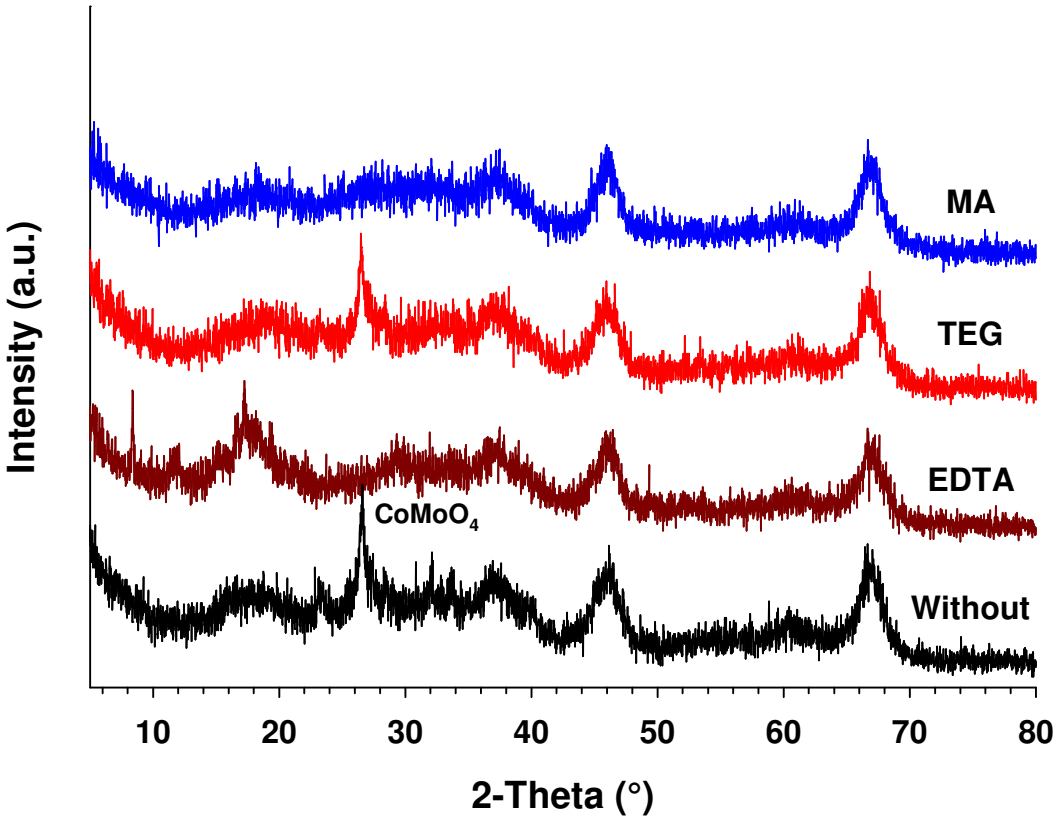

Bui et al.

Figure 2

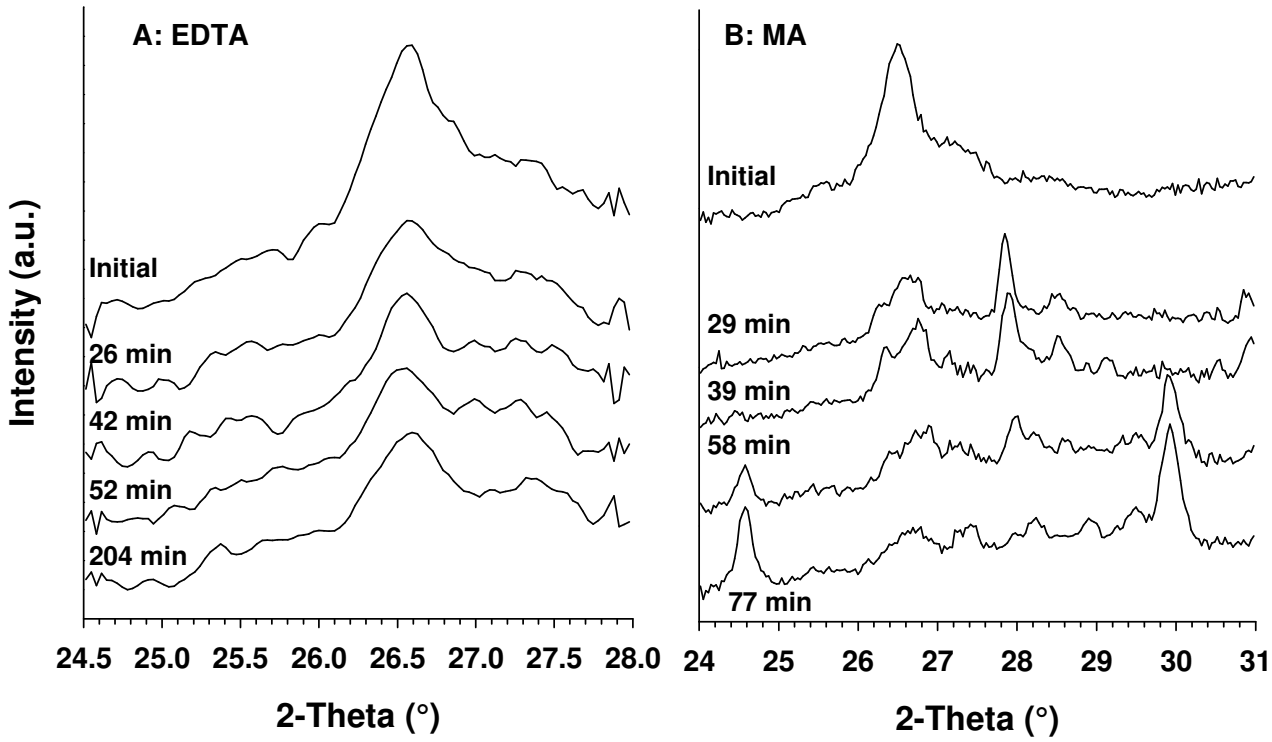

Bui et al.

Figure 3

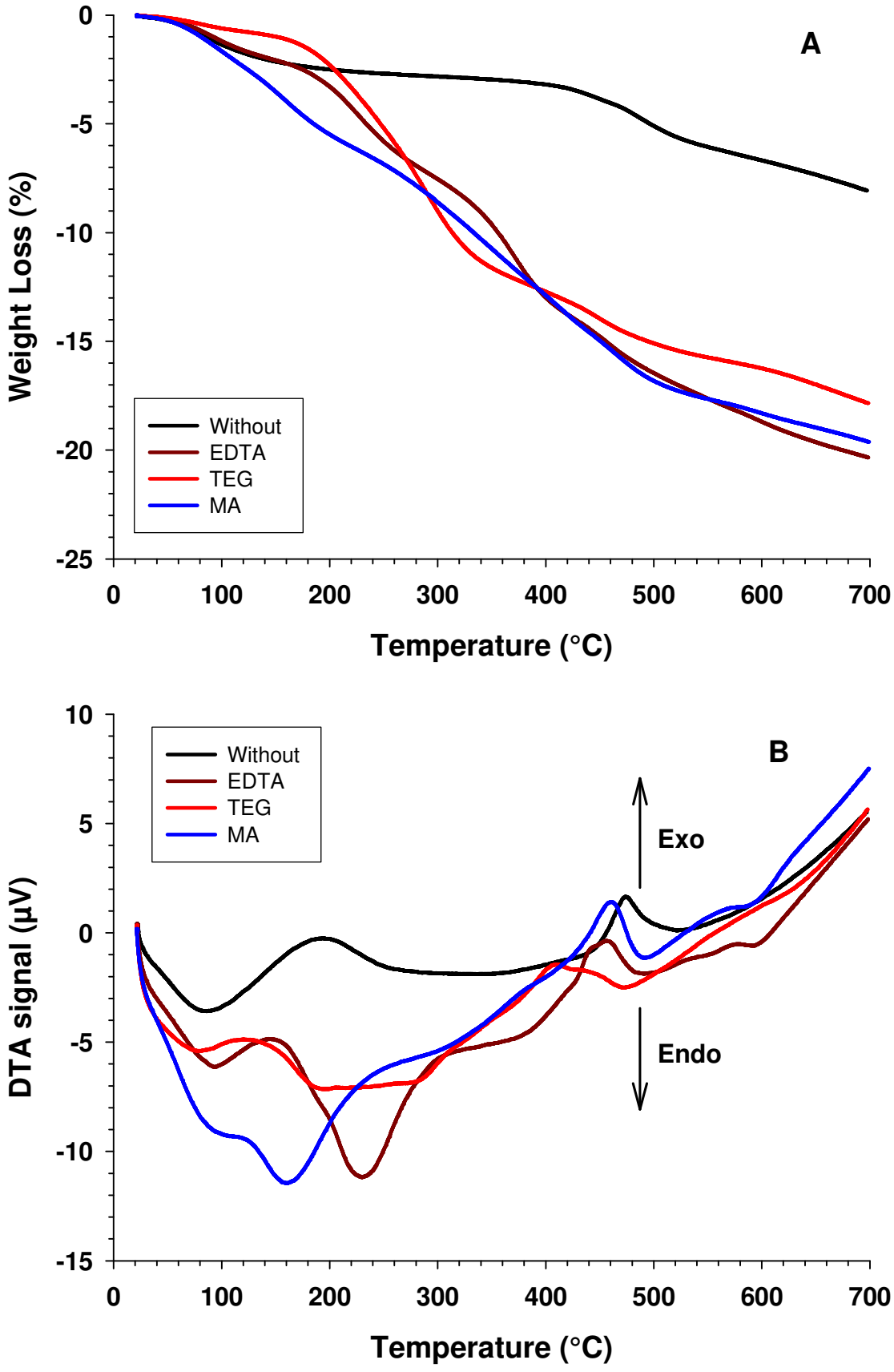

Bui et al.

Figure 4

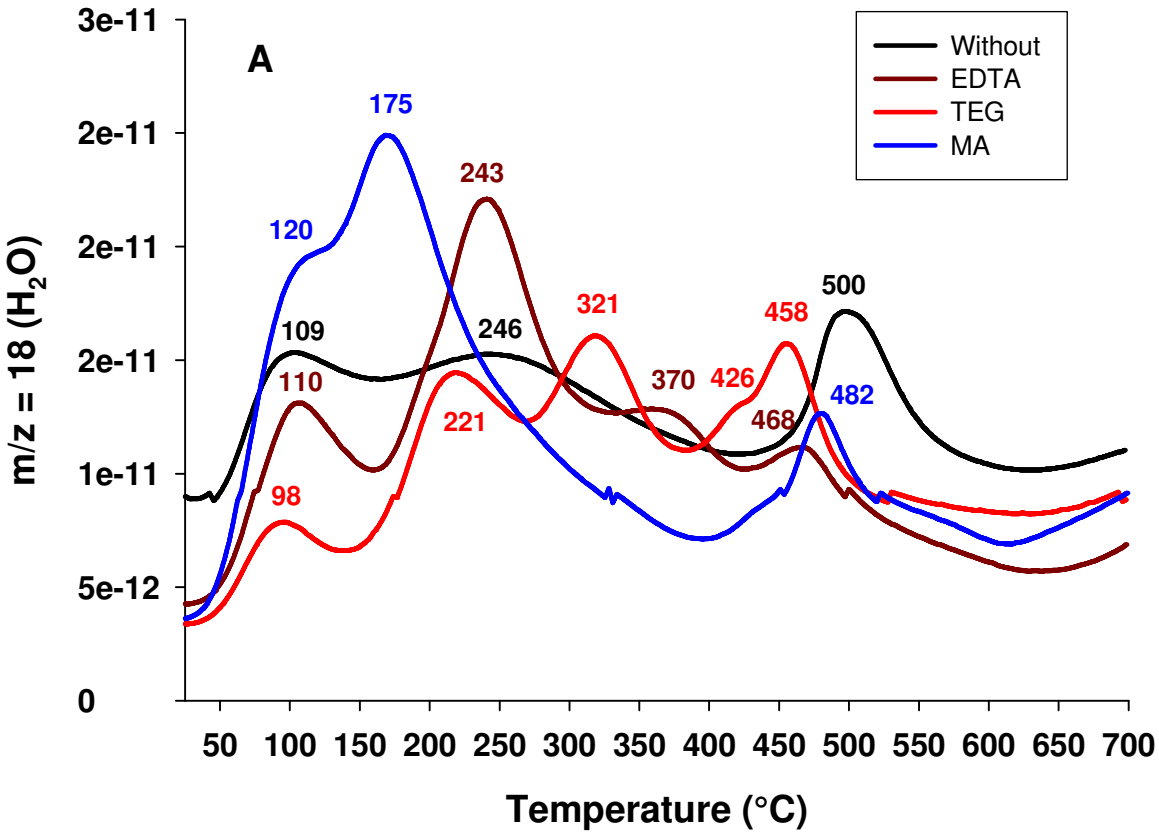

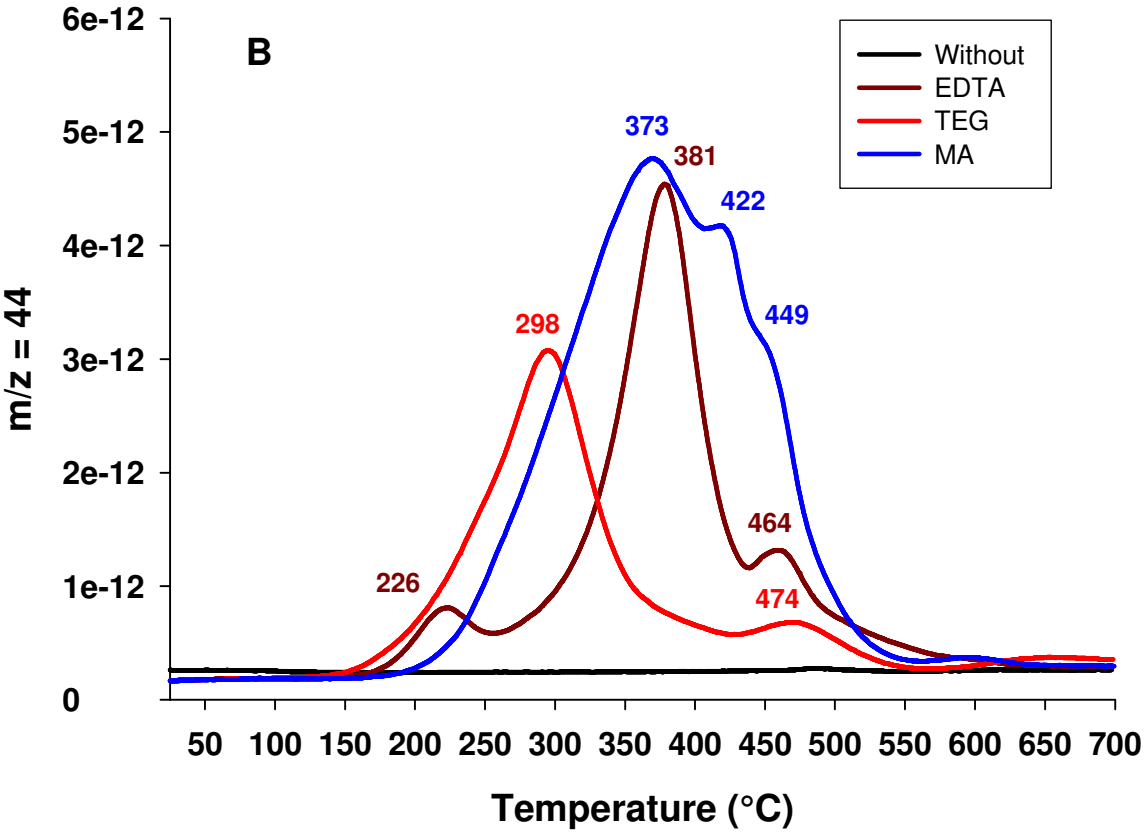

Bui et al.

Figure 5

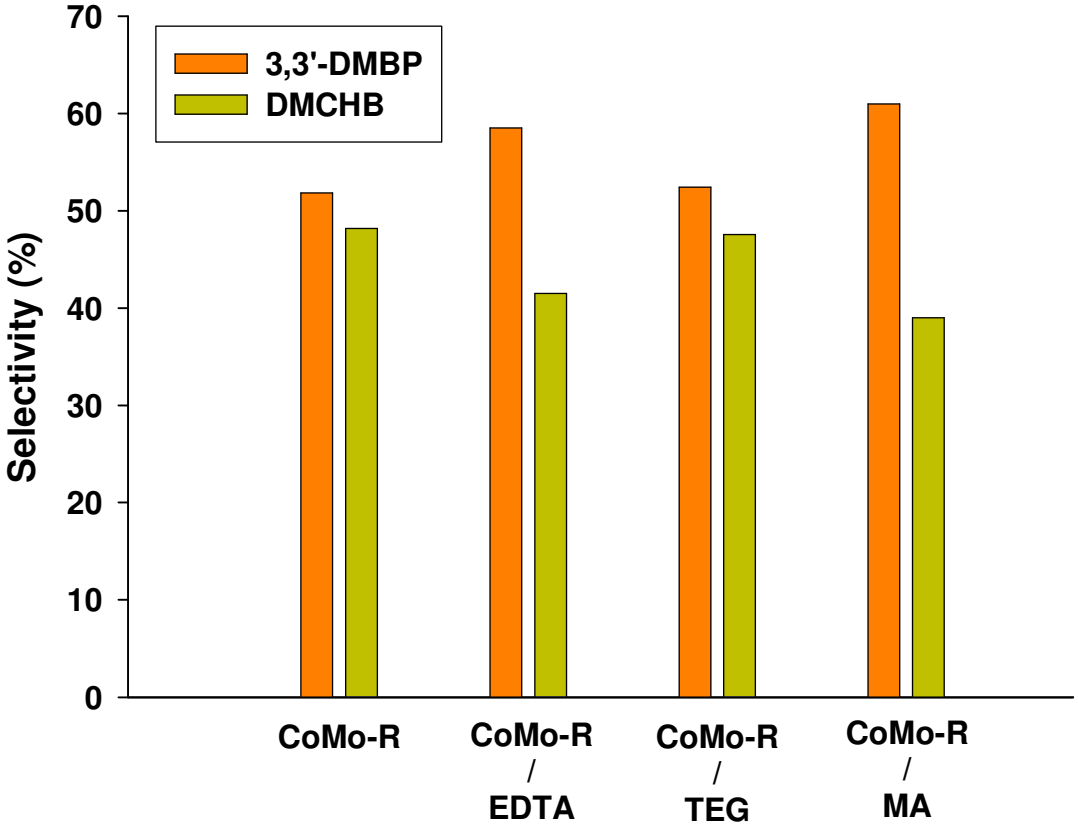

Bui et al.

Figure 6

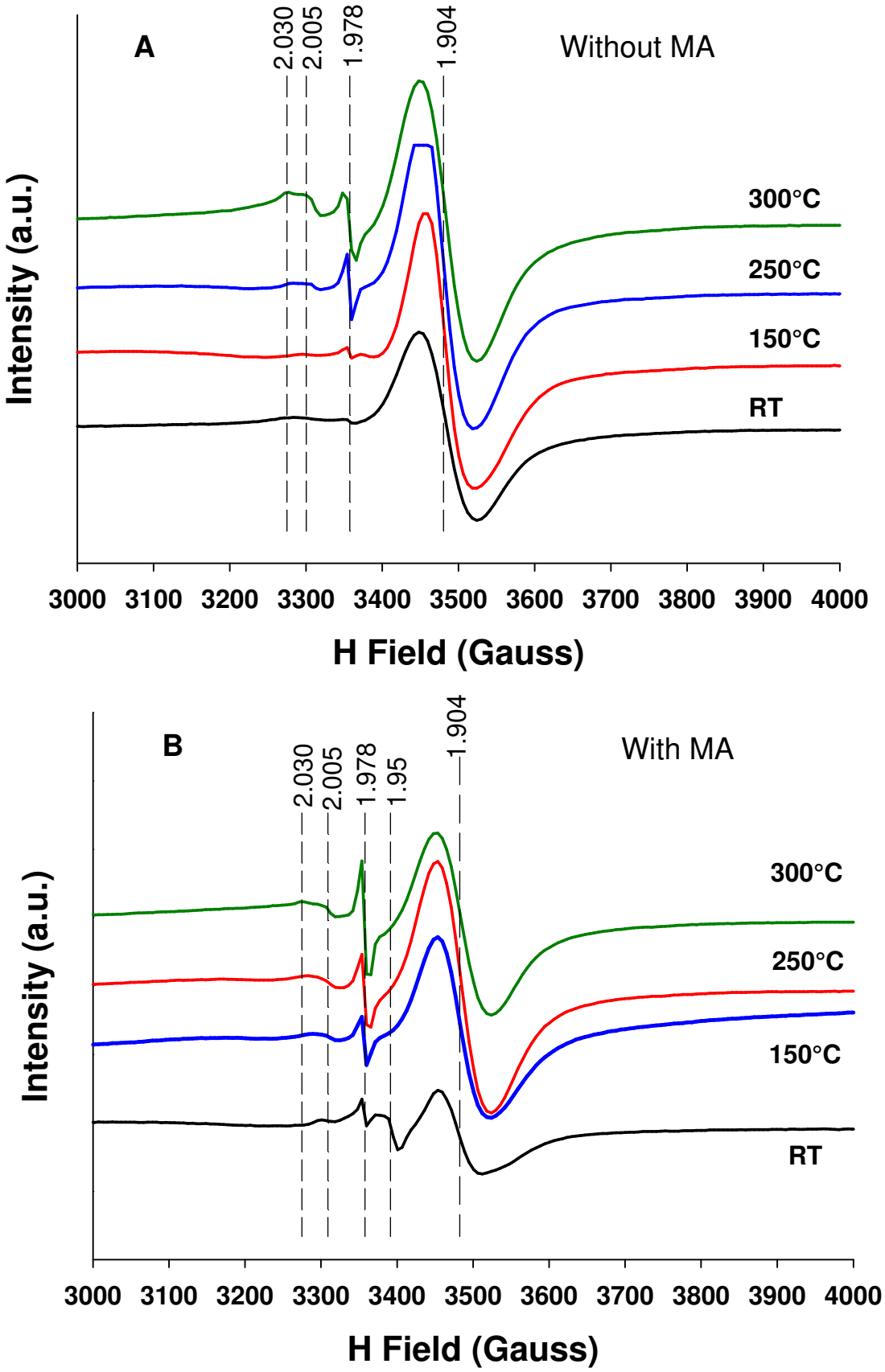

Bui et al.

Figure 7

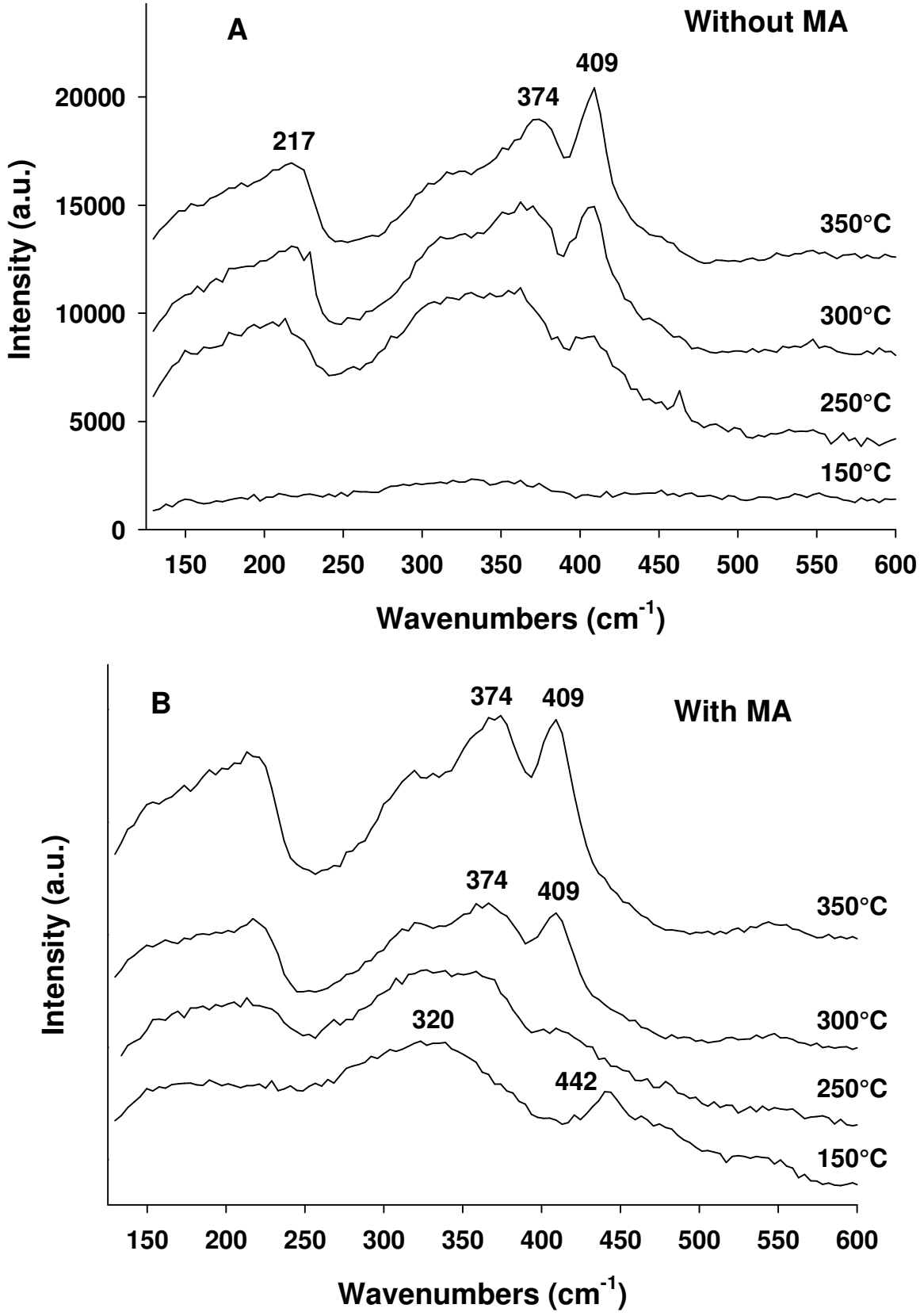

Bui et al.

Figure 8

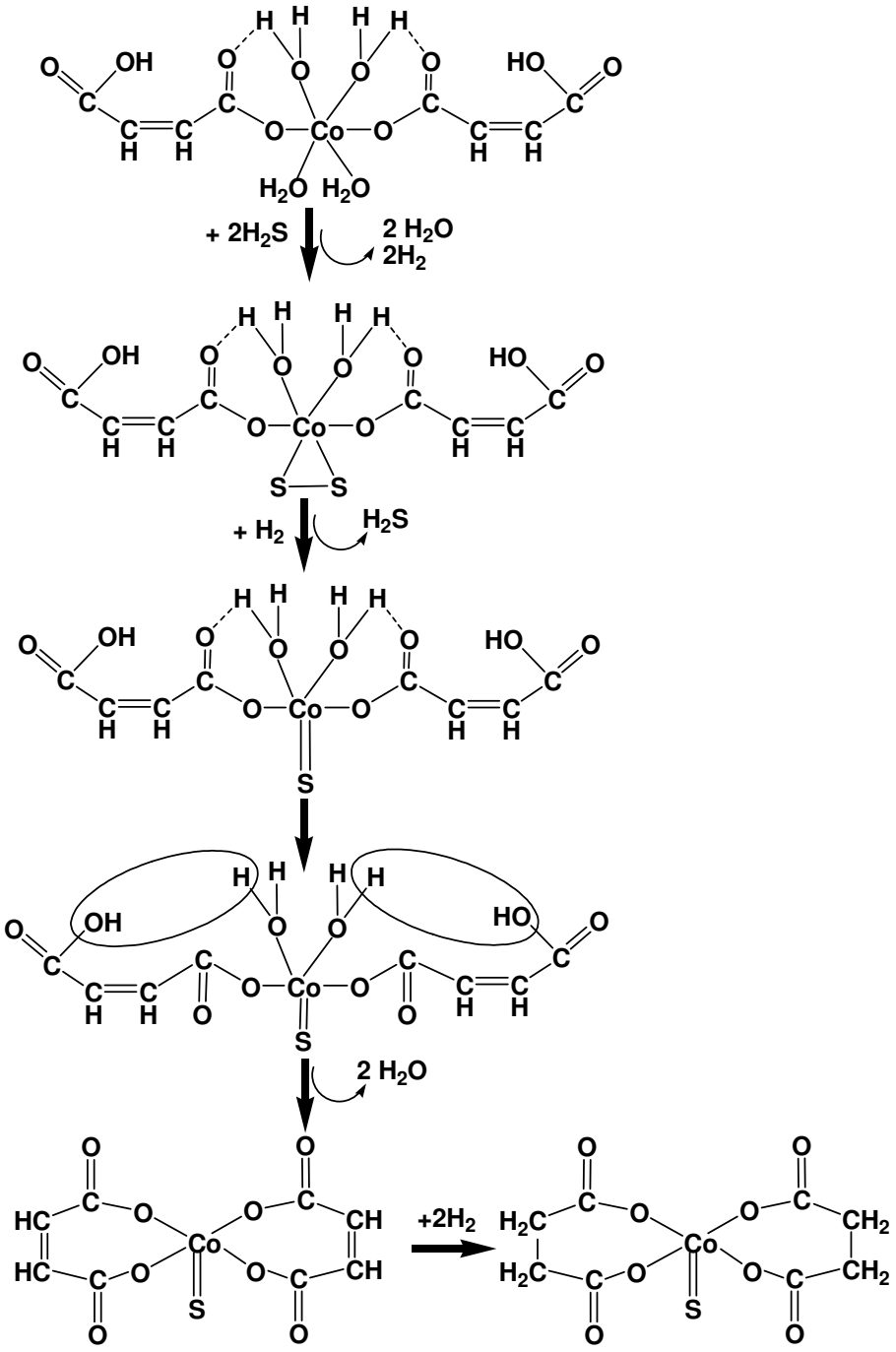

Bui et al.

Figure 9

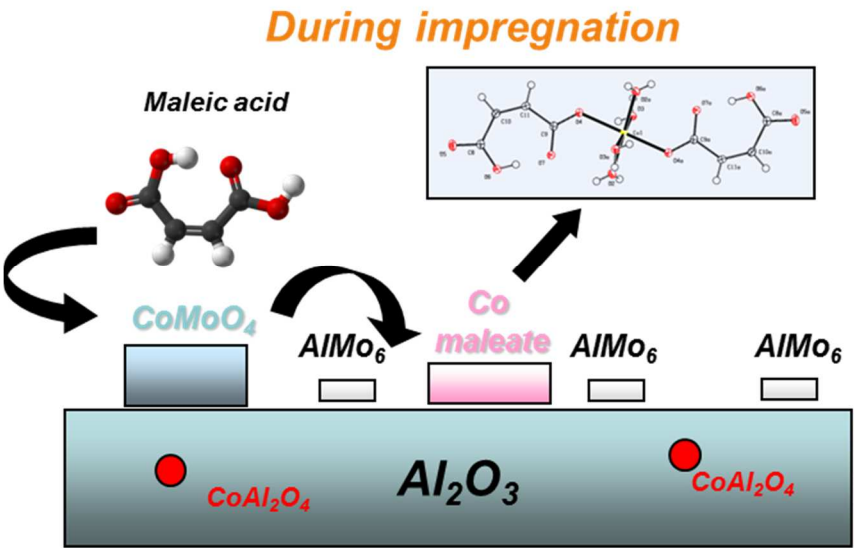

Steps 1 and 2: Selective interaction of maleic acid with Co if coming from $CoMoO_4$, no interaction with cobalt aluminate. The interaction of maleic acid with Co leads to the formation of cobalt maleate and the redispersion of Mo as $AlMo_6$ species.

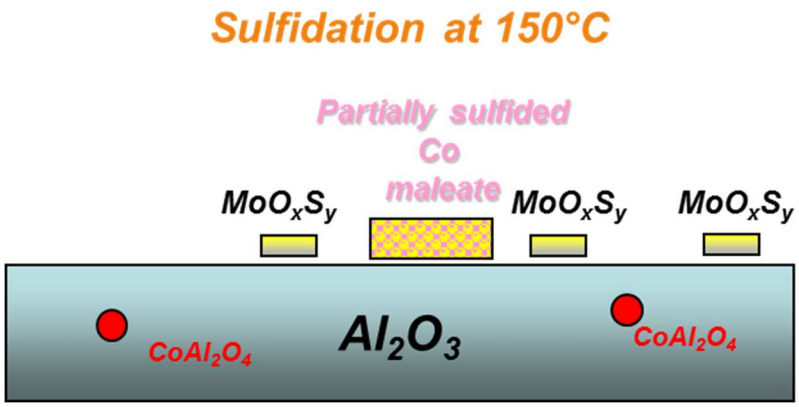

Step 3: Mo is rapidly sulfided forming well-dispersed oxysulfides. Co maleate is partially sulfided probably by replacement of the water ligands by S while keeping maleate coordinated.

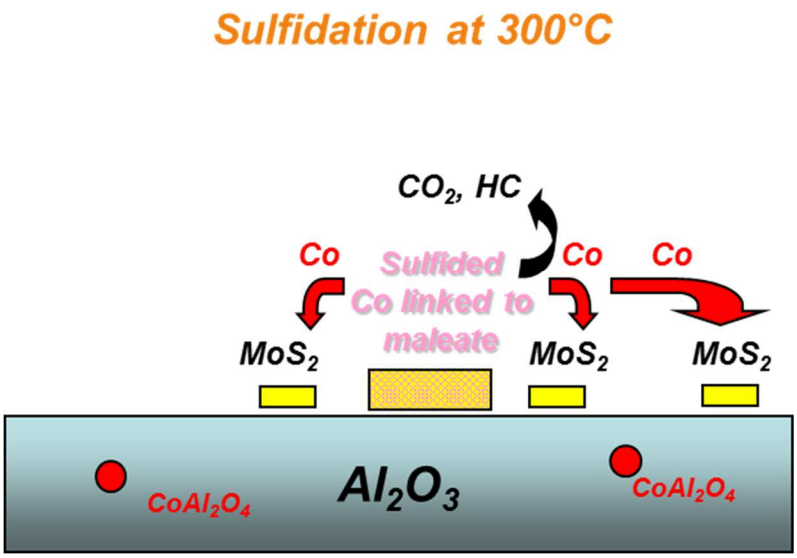

Step 4: sulfided Co linked to maleate ligands decomposes leading to the formation of CO_2 and hydrocarbons and liberating progressively cobalt while MoS_2 is already formed.

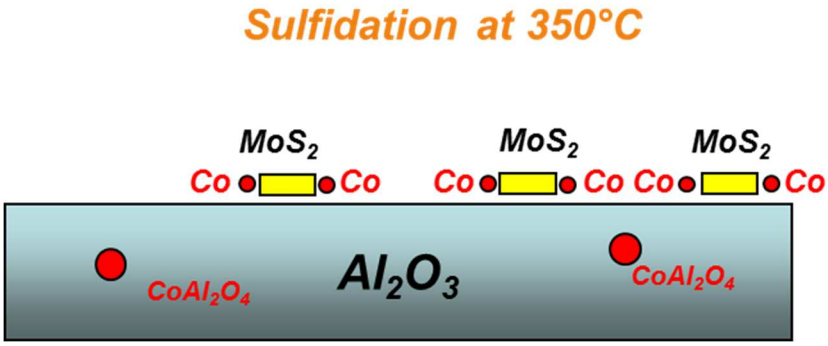

Step 5: the complete decomposition of maleate species makes cobalt available to interact with the edges of MoS_2 layers increasing the efficiency for the formation of the promoted CoMoS phase.

Bui et al.

Figure 10.

Table 1. Comparison between the temperatures of decomposition of free additives and the maximum temperature of decomposition (following the m/z = 44 fragment) after impregnation onto the regenerated $CoMo/Al_2O_3$ catalyst.

Additive	**Temperature of decomposition of the free additive (°C)**	**Maximum temperature of decomposition after impregnation (°C)**	**ΔT (°C)**
EDTA	218	381	163
TEG	285	298	13
MA	135	373	238

Table 2. Catalytic activities in the HDS of 4,6-dimethyldibenzothiophene performed at 300°C of the regenerated $CoMo/Al_2O_3$ catalyst prepared without or with organic additives (TEG, EDTA or MA).

Catalyst	**Reaction Rate (10^{-4} mol.g_{cat}^{-1}.h^{-1})**
$CoMo/Al_2O_3$	2.3
$CoMo/Al_2O_3$-EDTA	4.5
$CoMo/Al_2O_3$-TEG	3.3
$CoMo/Al_2O_3$-MA	4.2

Table 3. Residual sulfur amounts and rate constant k_{app} values (in $g^{0.2}.mmol^{-0.2}.h^{-1}$) for the regenerated $CoMo/Al_2O_3$ catalyst prepared without or with organic additives (EDTA, TEG, or MA) during the HDS of SRGO. Values are provided at three different temperatures of reaction (338°C, 343°C, and 348°C).

CoMo/ Al_2O_3 Catalysts	**Reaction Temperature (°C)**					
	338		**343**		**348**	
	S amount (ppm)	**Rate constant**	**S amount (ppm)**	**Rate constant**	**S amount (ppm)**	**Rate constant**
Without	557	10.8	398	12.4	190	16.4
EDTA	311	15.8	270	16.6	172	19.6
TEG	640	11.5	475	13.1	294	15.8
MA	199	18.4	103	23.0	52	28.4

Table 4. TEM Statistical analysis of the average slab length and stacking degree of the CoMo-R samples sulfided in the presence or not of the MA additive at 250°C, 300°C and 350°C.

Sulfidation Temperature (°C)	**250**		**300**		**350**	
	Without AM	With MA	Without MA	With MA	Without MA	With MA
Slab length (nm)	3.4	3.4	3.4	3.4	3.4	3.3
Stacking degree	2.1	2.2	2.3	2.0	2.0	2.0

Graphical Abstract